Journal of The Electrochemical Society, **151** (1) C19-C24 (2004)
0013-4651/2003/151(1)/C19/6/$7.00 © The Electrochemical Society, Inc.

An Exact Algebraic Solution for the Incubation Period of Superfill

D. Josell,[z] T. P. Moffat,[*] and D. Wheeler

Metallurgy Division, National Institute of Standards and Technology, Gaithersburg, Maryland, USA

Recent publications have used the impact of area change coupled with conservation of adsorbed catalyst to quantify the ''superfill'' effect of bottom-up feature filling during electrodeposition and chemical vapor deposition. This work describes how that superfilling process can be quantified using planar fronts that grow from corners where surfaces impinge. The results obtained apply only when catalyst is preadsorbed on the surface, with no subsequent accumulation or consumption. However, because they are exact solutions, they can also be used to check the accuracy of models and computer codes concerned with the more general problems of feature filling. Implications for sidewall deposition associated with the incubation period are discussed.
 [DOI: 10.1149/1.1626672]

Manuscript submitted February 11, 2003; revised manuscript received July 1, 2003. Available electronically November 26, 2003.

The implementation of copper electrodeposition for fabrication of metallizations in submicrometer circuitry has been successful because of the superconformal bottom-up feature filling, *i.e.*, ''superfill'', that is obtained with industrial electrolytes. The curvature enhanced accelerator coverage (CEAC) mechanism has been proposed to underlie this superconformal deposition process. It is described in a series of publications that have also detailed electrolytes for superconformal feature filling with both copper and silver.[1-4] The CEAC mechanism accounts for the impact of locally changing surface area on the coverage of adsorbates. It has been used to quantitatively predict superconformal feature filling during copper electrochemical deposition (ECD),[1,2] silver ECD,[3,4] and copper chemical vapor deposition (CVD).[5-7] The copper ECD process uses a catalyst that increases metal deposition rate and an inhibitor that decreases metal deposition rate; the other processes use only a catalyst. All the kinetics required for the feature filling predictions are obtained from studies on planar substrates.

Publications vary widely in the proposed role of adsorbates in superconformal feature filling during copper ECD. Some consider variations of traditional leveling models, specifically focusing on depletion of inhibitor.[8-11] Some propose competitive adsorption of various additives during copper ECD, subject to equilibrium between the adsorbed catalyst and the adjacent electrolyte.[12] Perhaps because of the comparative simplicity of the process, every publication about iodine-catalyzed copper CVD has suggested that the impact of area change on coverage of adsorbed catalyst underlies superconformal feature filling.[13-15] However, aside from the CEAC-based publications, only two papers include quantitative modeling of the impact of area change on coverage of adsorbates.[16,17] Both model copper ECD and fit the model predictions to feature filling experiments to obtain some kinetic parameters. One of these also invokes equilibrium coverage of adsorbed catalyst at the start of the simulations but then chooses to relax the boundary condition during feature filling.[17]

The computational complexities of published CEAC-based models vary substantially. Some models use level-set and scalar variable techniques to solve the full transport equations in the electrolyte and enforce the CEAC mechanism at the moving boundary within the filling feature.[18,19] These full solutions quantitatively predict all aspects of feature filling including incubation period, bottom-up fill, and overfill bump formation. They also capture void formation where failure to fill occurs. However, a single feature filling simulation takes upward of 10 h on a 1 GHz computer. Models of intermediate complexity use front tracking algorithms to account for geometrical compression of adsorbed catalyst, but neglect concentration variations within features.[1] Taking only a few minutes on the same computer, these models still provide accurate assessment of catalyst accumulation and feature filling, capturing the incubation period, bottom-up fill, and overfill bump formation.[18] Predicted failure to fill, however, manifests as seam formation rather than void formation. The simplest CEAC-based models evaluate feature filling using vertical sidewalls, a horizontal bottom, uniform distributions of catalyst on each surface, and an approximation of cupric depletion within the features.[2,20] Because each simulation requires less than 1 s, these simple models permit rapid examination of parameter space for approximate determination of the range of conditions that will yield feature filling.

Closed form, or otherwise precisely quantifiable, descriptions of feature filling that can be used to assess the accuracy of such codes have not existed. This is particularly significant because the features being filled have concave corners that can challenge the numerical implementations of most models. The solutions for superconformal filling of trenches presented in this work include exact results for feature filling over a wide range of conditions. Because exact solutions are obtained, these problems can be considered as test cases for evaluating the accuracy of codes meant to address feature filling under more general conditions.

The Solution

Geometry.—The problem addressed is that in which a given amount of catalyst has been preadsorbed on the surface of a trench prior to metal deposition. This technique has been used to achieve superconformal filling by copper ECD,[21] silver ECD,[22] and copper CVD.[5-7] In the modeling, there is assumed to be no accumulation, consumption, or diffusion of catalyst during the metal deposition. Figure 1 shows the geometrical evolution being considered: (a) superconformal metal deposition manifests first as growth of inclined surfaces from the bottom corners, (b) those surfaces impinge in the middle of the bottom surface, (c) a new bottom surface originates at the impingement site, (d) that new bottom surface eventually makes contact with the sidewalls. At that point, the geometry is that of the original rectangular trench; the inclined surfaces are expected to form again. The first stage of superconformal filling (from Fig. 1a to b) has been observed in numerous experiments, including some of the works already cited,[6,7,16,21] as well as in the predictions of various models.[1,3,5-7,16-18] The second stage (from Fig. 1b to d) has also been observed in experiments[6,7,16] and predictions.[1,3,5-7,18]

Quantifying the progression during the first stage of the incubation period (Fig. 1a to b) was accomplished by considering two positions of the interface (Fig. 2). Due to the symmetry of the problem, with identical catalyst coverage on the sidewall and bottom surfaces, the normal for the inclined surface was at $\pi/4$ as indicated. The two growth contours were considered to be separated in time by an infinitesimal increment of time Δt (we show that the results also hold for finite time increments). It was presumed that the length of the inclined section increased with time, so that the angle ψ_1 defining the motion of the intersection between the bottom and inclined

* Electrochemical Society Active Member.
[z] E-mail: daniel.josell@nist.gov

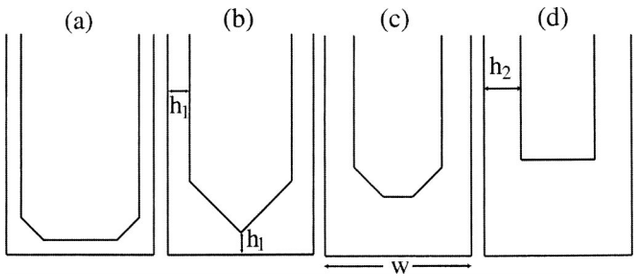

Figure 1. Schematics of superconformal feature filling: (a) inclined growth surface growing from the corner where the sidewall and bottom surfaces meet, (b) impingement of the surfaces coming out from the two lower corners, (c) new bottom surface growing from the corner where the inclined surfaces impinged, (d) elimination of the inclined surfaces by the new bottom surface.

surfaces satisfied $0 \leqslant \psi_1 \leqslant \pi/4$, as drawn; were this not the case, the new surface would not have formed. Spatially uniform catalyst coverages θ and normal velocities v were ascribed to each surface as per Fig. 2; note that this is self-consistent. The starting catalyst coverage θ_1 was presumed to be known and the deposition rate (*i.e.*, normal velocity) was presumed to depend only on the catalyst coverage θ through a function $v(\theta)$ that was also known [with $v_1 \equiv v(\theta_1)$ and $v_2 \equiv v(\theta_2)$]. Saturation of coverage θ is not considered here; *i.e.*, θ was not constrained to be less than unity. The distances moved by the inclined and bottom surfaces in Fig. 2 during the time increment Δt have been expressed using their normal velocities.

Solution for the first stage of the incubation period.—Invoking conservation of adsorbed catalyst leads to Eq. 1

$$d_1\theta_1 = d_2\theta_2 \qquad [1]$$

equating the quantity of catalyst adsorbed on the newly created section of the inclined surface with that which was on the eliminated section of bottom surface. As per Fig. 2, the lengths d_1 and d_2 can be expressed in terms of the velocities and the angle ψ_1

$$d_1 = v_1\Delta t/\tan(\psi_1)$$
$$d_2 = v_2\Delta t \tan\left(\frac{\pi}{4} - \psi_1\right) \qquad [2]$$

As a result, Eq. 1 becomes

$$\frac{\theta_1}{\theta_2} = \frac{v_2}{v_1}\tan(\psi_1)\tan\left(\frac{\pi}{4} - \psi_1\right) \qquad [3]$$

Also from Fig. 2, the equation for the bottom surface is

$$y = v_1\Delta t \qquad [4]$$

while that for the inclined surface is

$$y = -x + v_2\Delta t\sqrt{2} \qquad [5]$$

This yields the time-dependent intersection (x_1, y_1) of these surfaces

$$(x_1, y_1) = v_1\Delta t\left(\sqrt{2}\frac{v_2}{v_1} - 1, 1\right) \qquad [6]$$

Noting that $\tan(\psi_1) = \text{slope}(x_1, y_1)$, one obtains

$$\tan(\psi_1) = \left(\sqrt{2}\frac{v_2}{v_1} - 1\right)^{-1} \qquad [7]$$

Equation 3 and 7, with the definitions $v_1 \equiv v(\theta_1)$ and $v_2 \equiv v(\theta_2)$, represent two equations for the two unknowns ψ_1 and θ_2. Note that these equations continue to be satisfied during successive growth if they are already being satisfied. Thus, they can be used to define the growth of the incline and sidewalls from the start of deposition until impingement (Fig. 1b). This can be accomplished by replacing Δt by the time t elapsed since the start of deposition and invoking an infinitesimal corner at the start of metal deposition.

By symmetry, the inclined surfaces originating from the two bottom corners (Fig. 1b) meet at $x_1(t_1) = w/2$ (defining the time t_1 from the start of deposition to the contact of the two surfaces). Replacing Δt by t_1, Eq. 6 yields

$$t_1 = \frac{w/2}{v_1(\sqrt{2}v_2/v_1 - 1)} \qquad [8]$$

The deposit thickness h_1 on the sidewalls at the end of this stage of the incubation period (Fig. 1b) is then obtained by multiplying the deposition time t_1 by the deposition rate v_1

$$h_1 = v_1t_1 = \frac{w/2}{\sqrt{2}v_2/v_1 - 1} \qquad [9]$$

Alternatively, Fig. 2 yields the geometrical relationship

$$\frac{2h_1}{w} = \frac{2y_1(t_1)}{w} = \tan(\psi_1) \qquad [10]$$

That Eq. 9 and 10 are identical can be shown using the expression for $\tan(\psi_1)$ in Eq. 7.

Solution for the second stage of the incubation period.—The second stage of the incubation period is associated with the rapid upward motion of the bottom surface created when the two inclined surfaces first impinged (Fig. 3). Visual inspection of Fig. 2 and 3 shows that the second stage geometry is identical to the first stage geometry rotated by $\pi/4$ radians counterclockwise. Thus, the solution obtained for the first stage can be applied directly to determine

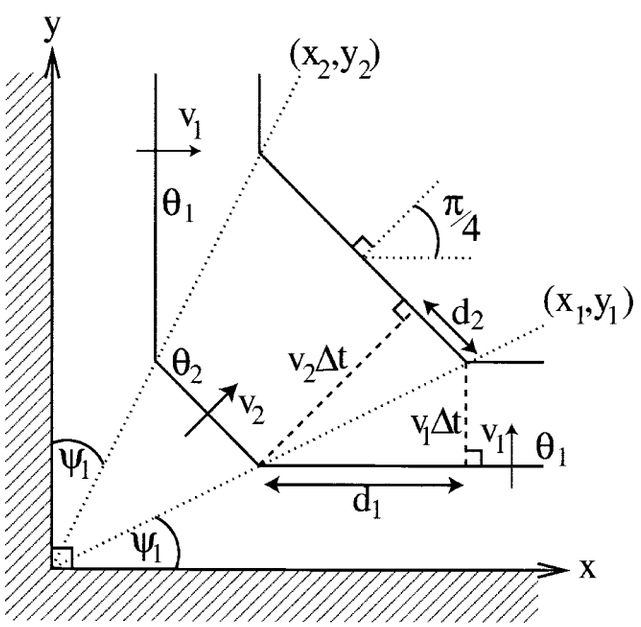

Figure 2. Schematic of the evolution of the growth surface coming from the lower left corner. Two growth contours representing the surface of the metal deposit at two times separated by time Δt are pictured. Parameters that define the geometry of the evolution are indicated.

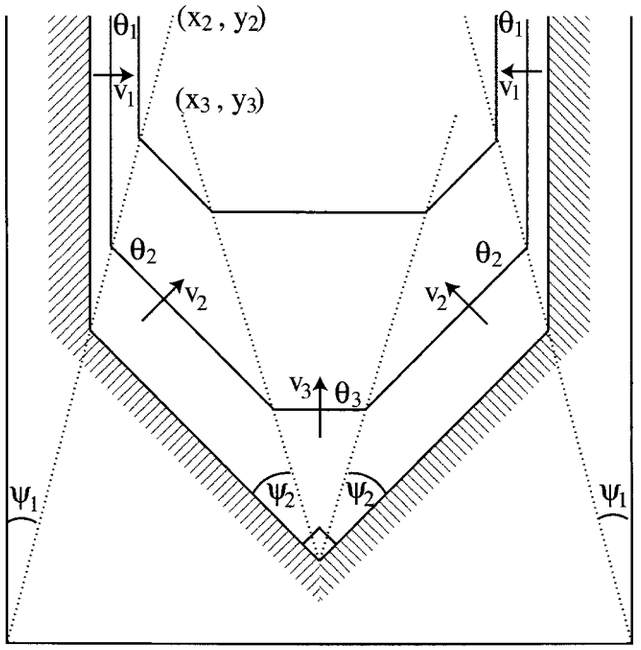

Figure 3. Schematic of the evolution of the new surface formed when the two inclined surfaces collided. Two growth contours representing the surface of the metal deposit at times separated by time Δt are pictured. Parameters that define the geometry of the evolution are indicated.

the coverage θ_3 and the angle ψ_2 that define the second stage by the variable changes $\theta_2 \rightarrow \theta_3$, $\theta_1 \rightarrow \theta_2$, and $\psi_1 \rightarrow \psi_2$ in Eq. 3 and 7 to obtain

$$\tan(\psi_2) = \left(\sqrt{2}\frac{v_3}{v_2} - 1 \right)^{-1} \qquad [11]$$

and

$$\frac{\theta_2}{\theta_3} = \frac{v_3}{v_2}\tan(\psi_2)\tan\left(\frac{\pi}{4} - \psi_2\right) \qquad [12]$$

As in the first stage, the coverages and velocities are uniform and constant on each segment throughout the second stage of the incubation period (from Fig. 1b to d).

From Fig. 3, the second stage of the incubation period ends where/when the line (x_2, y_2) defining the intersection between the sidewall and inclined surfaces meet the line (x_3, y_3) defining the intersection between the inclined and new bottom surfaces. The expression

$$(x_2, y_2) = v_1 t[1, 1/\tan(\psi_1)] \qquad [13]$$

can be obtained from the intersection of

$$x = v_1 t \qquad [14]$$

defining the sidewall and Eq. 5 defining the incline [using $\tan(\psi_1)$ found in Eq. 7]. The time t is again from the start of deposition. The expression

$$(x_3, y_3) = v_3(t - t_1)\left[-\tan\left(\frac{\pi}{4} - \psi_2\right), 1\right] + \left(\frac{w}{2}, h_1\right) \quad \text{for } t > t_1 \qquad [15]$$

was obtained from the geometry in Fig. 3. As with ψ_1, it is presumed that $\psi_2 < \pi/4$, consistent with formation of the new bottom surface when the inclined surfaces collide. The deposition time $t = t_2$ at which the upward moving bottom surface eliminates the inclined surfaces, achieving the state pictured schematically in Fig. 1d, is obtained by equating $x_2 = x_3$ to obtain

$$t_2 = \frac{v_3 t_1 \tan\left(\frac{\pi}{4} - \psi_2\right) + \frac{w}{2}}{v_1 + v_3 \tan\left(\frac{\pi}{4} - \psi_2\right)} \qquad [16]$$

The cumulative thickness of the sidewall deposit at the end of the second stage of the incubation period is then obtained from the product of the sidewall velocity and deposition time

$$h_2 = v_1 t_2 = \frac{v_3 t_1 \tan\left(\frac{\pi}{4} - \psi_2\right) + \frac{w}{2}}{1 + \frac{v_3}{v_1}\tan\left(\frac{\pi}{4} - \psi_2\right)} \qquad [17]$$

Implications of the results.—As per Eq. 9, the larger the ratio v_2/v_1 (*i.e.*, the smaller the angle ψ_1 from Eq. 7), the thinner the associated deposition on the sidewalls during the first stage of the incubation period. Thus, optimum filling is obtained if $v(\theta_1) \ll v(\theta_2)$. Substitution of this limiting condition in Eq. 3 and 7 yields $\psi_1 = 0$ (as expected) and $\theta_2/\theta_1 = \sqrt{2}$. Because $\psi_1 = 0$, there is negligible deposition on the sidewalls and bottom as the inclined surfaces advance inward. If $v(\theta_2) \ll v(\theta_3)$ is also satisfied, then Eq. 11 and 12 yield $\psi_2 = 0$ and $\theta_3/\theta_2 = \sqrt{2}$, and there also is negligible deposition on the sidewalls and incline as the bottom advances inward (after the inclined surfaces impinge). In both cases, ''negligible deposition'' means as a fraction of the feature width w.

While it is possible to obtain such behavior for some forms of $v(\theta)$, linear behavior of the form

$$v(\theta) = A + B\theta \qquad [18]$$

has been proposed for some processes.[5-7,15,23] For this case, Fig. 4 plots the scaled sidewall thickness $2h_1/w$ as a function of the ratio B/A (that is, as a function of just how strongly the adsorbed catalyst accelerates the metal deposition). The corresponding solutions for scaled catalyst coverage θ_2/θ_1 and deposition rate v_2/v_1 are also given. Representative values of v_2/v_1, θ_2/θ_1, and $2h_1/w$ can be found in Tables I and II. These results were obtained using the form $v(\theta)$ given in Eq. 18 and a starting coverage $\theta_1 = 0.05$, getting θ_2 and ψ_1 from Eq. 3 and 7, and then substituting in Eq. 10 for $2h_1/w$. Based on Fig. 4a, significant sidewall deposition cannot be avoided for linear $v(\theta)$; the deposit on each sidewall is a minimum of ≈20% of the feature width (thus, ≈40% combined). It may seem counterintuitive that this cannot be decreased as the impact of the catalyst on deposition rate is made arbitrarily large ($B/A \rightarrow \infty$). However, solution of Eq. 3 and 7 for this limiting case yields

$$\frac{v_2}{v_1} = \frac{\theta_2}{\theta_1} = \sqrt{2} + 1 \qquad [19]$$

and $\psi_1 = \pi/8$, giving $\tan(\psi_1) = \sqrt{2} - 1$. Equation 19 indicates that, for a linear velocity coverage relationship, the deposition rate on the incline does not exceed ≈2.41 times that on the sidewalls (and bottom), and Eq. 10 yields an associated value of $2h_1/w \approx 0.414$. As B/A decreases, θ_2/θ_1 increases monotonically, v_2/v_1 decreases monotonically, and the thickness of the sidewall deposit when the inclined surfaces impinge increases monotonically (Fig. 4a-c).

The sidewall thickness at the end of the second stage of the incubation period, as a function of B/A, is also overlaid in Fig. 4a; representative numerical values are given in Table II. The sidewall thickness is obtained using the expression

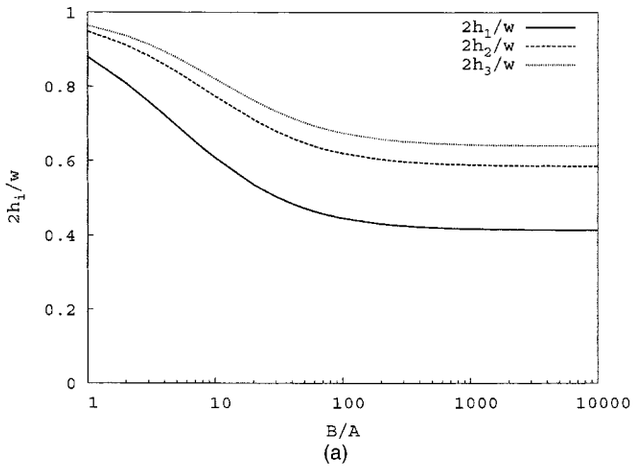

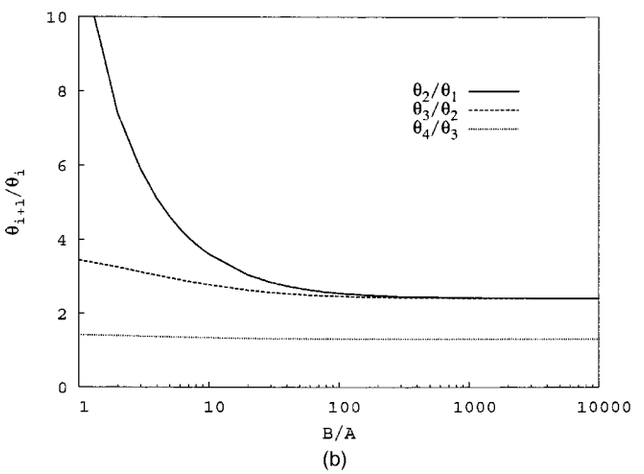

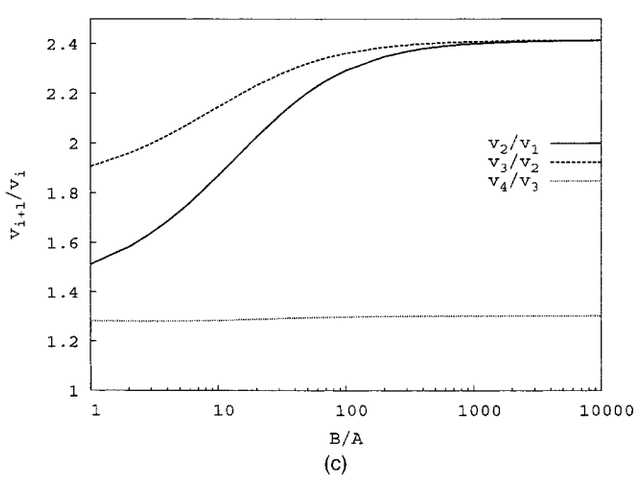

Figure 4. (a, top) The scaled thickness of the combined sidewall deposits at the end of each deposition stage as predicted for deposition rate-coverage relationship $v = A + B\theta$. (b and c) The associated coverage ratios and velocities ratios, respectively.

$$\frac{2h_2}{w} = \frac{\frac{v_3}{v_2}\frac{v_2}{v_1}\tan(\psi_1)\tan\left(\frac{\pi}{4} - \psi_2\right) + 1}{1 + \frac{v_3}{v_2}\frac{v_2}{v_1}\tan\left(\frac{\pi}{4} - \psi_2\right)} \quad [20]$$

which can be derived from Eq. 17, using Eq. 7 and 8. The inputs ψ_2 and v_3/v_2 were obtained from Eq. 11 and 12 using ψ_1 and v_2/v_1 obtained from solution of the first stage. The associated coverage and velocity ratios are also plotted in Fig. 4b and 4c, and representative numerical values are given in Table I. It is evident from both Fig. 4 and Table II that, for the linear velocity coverage relationship, the combined thickness of the deposits on the two sidewalls cannot be below ≈59% of the feature width. This result can be obtained by noting that, for the limiting case of $B/A \to \infty$ (*i.e.*, $v(\theta) = B\theta$)

$$\frac{v_2}{v_1} = \frac{v_3}{v_2} = \frac{\theta_2}{\theta_1} = \frac{\theta_3}{\theta_2} = \sqrt{2} + 1 \quad [21]$$

and $\psi_1 = \psi_2 = \pi/8$, so that $2h_2/w = 2/(\sqrt{2} + 1) \approx 0.586$.

Beyond the incubation period.—It is actually disingenuous to call the two stages of fill described above the ''incubation period'', because deposition is never truly conformal (in contrast to feature filling when catalyst accumulates from the electrolyte during metal deposition). As such, there is no reason that the formalism used is limited to studying these first two stages. Indeed, the geometry reached at the end of the incubation period (Fig. 1d) is just a smaller, higher aspect ratio version of that existing at the start of feature filling. Therefore, one might again expect the formation of inclined surfaces where the sidewall and bottom surfaces meet.

However, because the bottom surface has a different coverage than that on the sidewall, there is no longer a symmetry that forces the inclined surface to have a normal at an angle of $\pi/4$ (Fig. 5). Such surfaces, with normals at angles closer to $\pi/2$, have been observed in previous predictions.[5,18] Obtaining the geometry of the new inclined surface is straightforward. A mass conservation equation and a geometrical consistency equation (analogous to Eq. 3 and 7) can be written for the intersection of the new surface and sidewall as well as for the intersection of the new surface and bottom surface. The resulting four equations can then be solved for the four unknowns: the coverage on the incline θ_4, the angle defining the normal to the incline ψ_5, and the two angles ψ_3 and ψ_4 describing the evolution of bottom-incline and sidewall-incline intersections, respectively (Fig. 5).

To derive the four equations, first note that the sidewall and incline can be expressed as

$$x = \Delta t^* v_1 \quad [22]$$

and

$$y = -\frac{x}{\tan(\psi_5)} + \frac{v_4 \Delta t^*}{\sin(\psi_5)} \quad [23]$$

respectively; for simplicity, time Δt^* is relative to the end of the second stage of the incubation period and the origin is at the lower left corner of the corresponding unfilled region (width $w^* = w - 2h_2$). Using Eq. 22 and 23, one can obtain the line

$$(x_5, y_5) = \Delta t^* \left(v_1, \frac{v_4}{\sin(\psi_5)} - \frac{v_1}{\tan(\psi_5)} \right) \quad [24]$$

parametrized by Δt^*. The line

$$(x_4, y_4) = \Delta t^* \left(\frac{v_4}{\cos(\psi_5)} - \tan(\psi_5) v_3, v_3 \right) \quad [25]$$

also parametrized by Δt^* can be obtained from the intersection of the bottom

$$y = \Delta t^* v_3 \quad [26]$$

and inclined (Eq. 23) surfaces.

For consistency of the surface velocities and angles at the sidewall-incline and incline-bottom intersections, it is necessary that

Table I. Catalyst coverages obtained through solution of the relevant conservation and geometrical consistency equations for velocity that depends linearly on coverage. For all derivations, a value of $\theta_1 = 0.05$ was used (the value used only shifts the behavior as a function of B/A). Limiting values ($B/A \gg 1$) are discussed in the text.

B/A	θ_2/θ_1	θ_3/θ_2	θ_4/θ_3	ψ_3 (rad)	ψ_4 (rad)	ψ_5 (rad)
1	11.7335	3.44923	4.90162	0.725042	1.29649	1.27975
5	4.62723	2.97038	4.04882	0.703569	1.34936	1.29727
10	3.60931	2.78089	3.72925	0.690801	1.37604	1.30308
50	2.68316	2.51748	3.30523	0.666686	1.42012	1.30841
100	2.55186	2.46902	3.23008	0.661194	1.42922	1.30882
500	2.44233	2.42576	3.16382	0.655955	1.43761	1.30899
1000	2.42831	2.42003	3.15509	0.655235	1.43874	1.30899
5000	2.41704	2.41538	3.14804	0.654647	1.43966	1.30900
10000	2.41562	2.41479	3.14715	0.654573	1.43978	1.30900

$$\tan(\psi_3) = \text{slope}(x_4, y_4) \quad [27]$$

and

$$\tan(\psi_4) = \text{slope}(x_5, y_5) \quad [28]$$

Using the forms for (x_4, y_4) and (x_5, y_5) obtained in Eq. 25 and 24, Eq. 27 and 28 yield

$$\tan(\psi_3) = \left(\frac{v_4}{v_3}\frac{1}{\cos(\psi_5)} - \tan(\psi_5)\right)^{-1} \quad [29]$$

and

$$\tan(\psi_4) = -\frac{1}{\tan(\psi_5)} + \frac{v_4/v_1}{\sin(\psi_5)} \quad [30]$$

respectively. Invoking conservation of the adsorbed catalyst at the sidewall-incline and the incline-bottom intersections, (*e.g.*, see Eq. 1, 2 and 3) yields the two equations

$$v_1\theta_1 \tan(\psi_4) = v_4\theta_4 \tan(\psi_4 - \psi_5) \quad [31]$$

and

$$v_4\theta_4 \tan(\psi_5 - \psi_3) = \frac{v_3\theta_3}{\tan(\psi_3)} \quad [32]$$

respectively. Equation 29 through 32 permit the unknown quantities θ_4, ψ_3, ψ_4, and ψ_5 to be evaluated. The increment of sidewall deposition associated with this stage alone can then be obtained by using Eq. 25 to find the time increment Δt^* at which $x_4 = w^*/2$ and multiplying that value by the sidewall velocity v_1. The total thickness of the deposit at the end of this stage can then be written

$$\frac{2h_3}{w} = \frac{2h_2}{w} + \left(1 - \frac{2h_2}{w}\right)\left(\frac{v_4}{v_1}\frac{1}{\cos(\psi_5)} - \frac{v_3}{v_1}\tan(\psi_5)\right)^{-1} \quad [33]$$

Results for $2h_3/w$ and the coverage and velocity ratios are found in Fig. 4; representative numerical values for θ_4, ψ_3, ψ_4, ψ_5, and $2h_3/w$ are given in Tables I and II. Because of the relatively high deposition rate (*i.e.*, catalyst coverage) on the incline and the high value of ψ_5, there is relatively little additional sidewall deposition associated with this stage. Predictions obtained using the string model of Ref. 1 with both $B/A = 10$ and 100 show excellent agreement with the results in Tables I and II (demonstrating the accuracy of that code).

Extendability of the formalism.—The sidewalls of real features are frequently nonvertical. The formalism presented above can be applied to derive the catalyst coverages, deposition rates, and resulting fill dimensions for this geometry as well. The solution obtained also applies for simulation of deposition beyond the three stages already presented because the inclined surfaces in the third stage do not form a right angle where they impinge ($\psi_5 \neq \pi/4$). Because of its similarity to what has been presented, the derivation is omitted.

Table II. Combined sidewall thicknesses as a fraction of the feature width obtained using the catalyst coverages obtained in Table I for velocity that depends linearly on coverage. Limiting values ($B/A \gg 1$) are discussed in the text.

B/A	$2h_1/w$	$2h_2/w$	$2h_3/w$
1	0.879472	0.948639	0.964442
5	0.694371	0.839303	0.877719
10	0.608177	0.773634	0.820273
50	0.472931	0.648848	0.702914
100	0.445811	0.620410	0.674927
500	0.420958	0.593312	0.647889
1000	0.417615	0.589591	0.644149
5000	0.414898	0.586554	0.641092
10000	0.414556	0.586170	0.640705

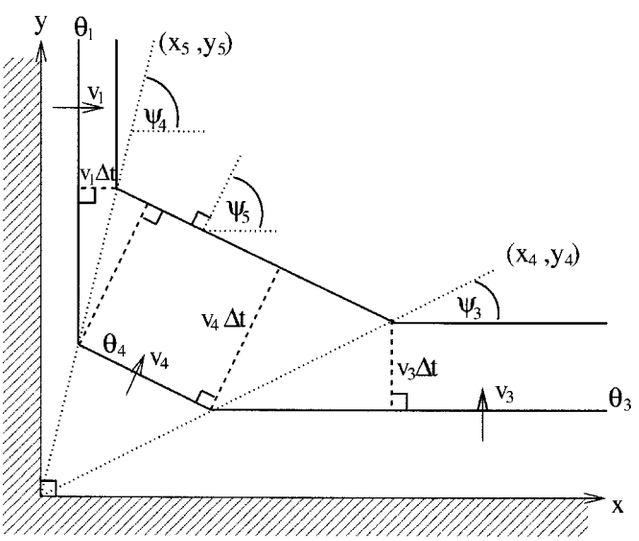

Figure 5. Evolution of deposition after the two stages of the incubation period. The new surface originates where the original sidewall and new bottom surfaces impinge. Two growth contours representing the surface of the deposit at times separated by time Δt are pictured. Parameters that define the geometry of the evolution are indicated.

Conclusion

It has been shown that, when catalyst has been preadsorbed on the surface of a trench, the superfilling process can be described using growth fronts that grow from corners where two surfaces impinge. The equations obtained are exact. They can be used to check the accuracy of models and computer codes concerned with the more general problems of feature filling. To aid in such checks, numerical values have been provided for representative cases where the deposition rate is linear in catalyst coverage. Limiting values, corresponding to the case that deposition rate is proportional to catalyst coverage, were also given. Among the significant results obtained is the existence of minimum sidewall thickness when deposition rate is linear in the catalyst coverage.

The National Institute of Standards and Technology assisted in meeting the publication costs of this article.

References

1. T. P. Moffat, D. Wheeler, W. H. Huber, and D. Josell, *Electrochem. Solid-State Lett.*, **4**, C26 (2001).
2. D. Josell, D. Wheeler, W. H. Huber, J. E. Bonevich, and T. P. Moffat, *J. Electrochem. Soc.*, **148**, C767 (2001).
3. T. P. Moffat, B. Baker, D. Wheeler, J. E. Bonevich, M. Edelstein, D. R. Kelly, L. Gan, G. R. Stafford, P. J. Chen, W. F. Egelhoff, and D. Josell, *J. Electrochem. Soc.*, **149**, C423 (2002).
4. B. C. Baker, M. Freeman, B. Melnick, D. Wheeler, D. Josell, and T. P. Moffat, *J. Electrochem. Soc.*, **150**, C61 (2003).
5. D. Josell, D. Wheeler, and T. P. Moffat, *Electrochem. Solid-State Lett.*, **5**, C44 (2002).
6. D. Josell, S. Kim, D. Wheeler, T. P. Moffat, and S. G. Pyo, *J. Electrochem. Soc.*, **150**, C368 (2003).
7. S. G. Pyo, S. Kim, D. Wheeler, T. P. Moffat, and D. Josell, *J. Appl. Phys.*, **93**, 1257 (2003).
8. D. Roha and U. Landau, *J. Electrochem. Soc.*, **137**, 824 (1990).
9. P. C. Andricacos, C. Uzoh, J. O. Dukovic, J. Horkans, and H. Deligianni, *IBM J. Res. Dev.*, **42**, 567 (1998).
10. A. C. West, *J. Electrochem. Soc.*, **147**, 227 (2000).
11. M. Hayase, M. Taketani, K. Aizawa, T. Hatsuzawa, and K. Hayabusa, *Electrochem. Solid-State Lett.*, **5**, C98 (2002).
12. Y. Cao, P. Taephaisitphongse, R. Chalupa, and A. West, *J. Electrochem. Soc.*, **148**, C466 (2001).
13. H. Park, W. Koh, S.-M. Choi, K.-C. Park, H.-K. Kang, J.-T. Moon, K. Shim, H. Lee, O. Kwon, and S. Kang, in *Proceedings of The IEEE 2001 International Technology Conference*, p. 12 (June 2001).
14. S. G. Pyo, W. S. Min, H. D. Kim, S. Kim, T. K. Lee, S. K. Park, and H. C. Sohn, in *Proceedings of the Advanced Metallization Conference*, AMC 2001, p. 209, Materials Research Society, Warrendale, PA (2002).
15. K.-C. Shim, H.-B. Lee, O.-K. Kwon, H.-S. Park, W. Koh, and S.-W. Kang, *J. Electrochem. Soc.*, **149**, G109 (2002).
16. A. C. West, S. Mayer, and J. Reid, *Electrochem. Solid-State Lett.*, **4**, C50 (2001).
17. Y. H. Im, M. O. Bloomfield, S. Sen, and T. S. Cale, *Electrochem. Solid-State Lett.*, **6**, C42 (2003).
18. D. Wheeler, D. Josell, and T. P. Moffat, *J. Electrochem. Soc.*, **150**, C302 (2003).
19. D. Josell, D. Wheeler, W. H. Huber, and T. P. Moffat, *Phys. Rev. Lett.*, **87**, 016102 (2001).
20. D. Josell, D. Wheeler, and T. P. Moffat, *Electrochem. Solid-State Lett.*, **5**, C49 (2002).
21. T. P. Moffat, D. Wheeler, C. Witt, and D. Josell, *Electrochem. Solid-State Lett.*, **5**, C110 (2002).
22. B. C. Baker, C. Witt, D. Wheeler, D. Josell, and T. P. Moffat, *Electrochem. Solid-State Lett.*, **6**, C67 (2003).
23. G. B. McFadden, S. R. Coriell, T. P. Moffat, D. Josell, D. Wheeler, W. Schwarzacher, and J. Mallett, *J. Electrochem. Soc.*, **150**, C591 (2003).